Front. Optoelectron. China 2010, 3(1): 84–91
DOI 10.1007/s12200-009-0078-9

REVIEW ARTICLE

Progress in creating second-order optical nonlinearity in silicate glasses and waveguides through thermal poling

Simon FLEMING (✉), Honglin AN

Institute of Photonics and Optical Science, School of Physics, University of Sydney, Sydney, NSW 2006, Australia

Abstract This paper describes progress in characterizing the distribution and localization of the second-order nonlinearity induced in thermally poled silicate glasses and optical waveguides, in particular, optical fibers. It starts by describing the basics of the poling technique, especially the most commonly used "thermal poling" technique. Then results of systematic investigation of the distribution of the second-order nonlinearity in poled glass and special fibers using second-harmonic microscopy are presented. Interesting issues such as the effectiveness of the poling technique for waveguides formed by ultrafast laser pulses are also discussed.

Keywords poling, silica, nonlinearity

1 Introduction

Silicate optical glasses are technologically very important materials, especially in telecommunications, because of their excellent properties such as strength, the ability to be drawn into fiber, and optical properties, including high transparency over a wide wavelength range. Silica glass has now become the backbone of modern communications systems. But its use has been confined to mainly passive roles due to its low nonlinearity.

In 1991, Myers et al. published the surprising result of creating a large second-order nonlinearity (SON) of the order of 1 pm/V in fused silica with a technique called "thermal poling" [1]. Since then, extensive research efforts have been put into further developing this technique, understanding the underlying mechanism, and applying this technique to other optical glasses. Over the last decade, the mechanism has been steadily elucidated, although much still needs to be understood for the process to be applied reliably and optimally. The thermal poling process involves the depletion of positive charges (mainly sodium ions, Na^+), which are made mobile by the heat and applied electric field, from a narrow region beneath anode and subsequent creation of an internal space-charge field with the migrated charges frozen into the glass after the heat is removed [2]. The internal space-charge field then acts on the third-order nonlinearity of the poled glass to give a second-order nonlinearity to the otherwise amorphous glass [3].

Other poling techniques have also been demonstrated, including UV poling [4], corona poling of glass films [5], e-beam poling of lead silicate glass [6], and proton implantation [7]. Of all these, thermal poling remains the most reliable and widely used method.

Received August 1, 2009; accepted August 30, 2009

E-mail: s.fleming@usyd.edu.au

2 SON characterization

2.1 SON characterization methods

A frequently used method for investigating the location of the SON is etching the thermally poled silica plates or optical fibers with hydrofluoric acid (HF). Due to etching rate change in the presence of a strong electric field and/or charges, the spatial distribution of the frozen-in space-charge field can be revealed from such experiments [8]. By gradually removing glass material from the anode side and, at the same time, monitoring second-harmonic (SH) signal from the etched sample, the depth of the depletion layer in bulk samples can also be measured [9]. Later, a layer-peeling technique was applied to HF measurements that were interferometrically monitored to achieve sub-micron resolution characterization of the spatial distribution of the nonlinear region [10]. These studies provided strong support for the charge migration models that were being developed at this time.

However, a serious drawback to this HF etching method is that it cannot distinguish between contributions to the HF etching rate change from changes of electric field and

charge densities, which are both present in the SON layer. The etching rate is also altered by Ge doping in the fiber core and stress at the core-cladding interface due to the difference in fiber core and cladding materials.

An important advance in measuring the location and movement of the SON was the application of SH microscopy to poled glass samples [11], which were cut parallel to the direction of the applied electric field to expose the cross section. The surface of the cut sample was further polished to optical finish. The excitation laser source is a Coherent Verdi-Mira tunable pulsed titanium sapphire laser with a wavelength of 830 nm and pulses in the 100–200 fs range. The microscope is equipped with dual photomultiplier transmitted light detectors, with a 505 dichroic long-pass (DCLP) dichroic mirror dividing the detectable spectrum (380–680 nm) at 505 nm between the two channels; the shorter wavelength channel receives only the SH, and the longer wavelength channel detects the range from 505 to 650 nm, including a wide-range two-photon fluorescence and, in some cases, a transmitted non-confocal image using the 543-nm green helium-neon laser.

This SH microscopy technique can measure the spatial distribution of the induced SON no matter what the mechanism is. It is also suitable for samples with irregular geometrical shapes, like optical fibers, which cannot be characterized with the traditional Maker fringe method [1]. We apply this technique extensively to a number of bulk and fiber glass samples.

2.2 SON in fused silica

A typical result from a sample thermally poled at 4 kV and 250°C for 30 min is shown in Fig. 1. The channel 1 image (Fig. 1(a)) shows the area where the SH microscopy was conducted; the interface between the anode surface (on the left side) and the glued supporting microscope slide can be clearly seen. The SH signal from channel 2 is shown in Fig. 1(b). A bright straight line can be seen just on the poled silica, corresponding to a well-defined SON spatial distribution. Some discontinuity along the line can also be observed, believed to be mainly due to the inhomogeneities in the poled fused silica.

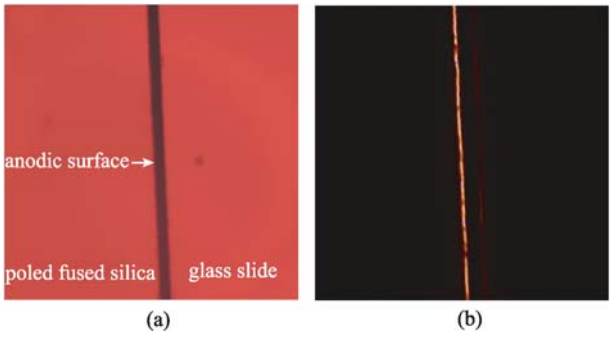

Fig. 1 SH micrographs of cross-section of a fused silica sample thermally poled at 4 kV and 250°C for 30 min. (a) Channel 1; (b) channel 2

To obtain the SON profile, a line scan across the SON layer was performed. For every point along the scanning line, the detected SH signal is related to the SON through $P(2\omega) \propto (P(\omega)\chi^{(2)})^2$, where $\chi^{(2)}$ is the second-order nonlinear susceptibility. Therefore, the SON spatial profile can be obtained by taking the square root of the measured SH signal, as shown in Fig. 2. The SON profile is asymmetrical, increasing more sharply at the anode side, reaching the maximum value and then tailing away deeper into the sample. This can be explained by charge transport during the poling process. The frozen-in field is now generally believed to be formed between externally injected hydrogenated species such as H^+ or H_3O^+ and those immobile negative charges left behind in the depletion region, after the mobile cations (e.g., Na^+) have migrated to the cathode. Under the assumption of a narrow line distribution for the injected hydrogenated species and a wider depletion region with approximately constant negative charge density N, the electric field predicted by theory should abruptly reach its peak value and then decrease linearly with a slope of eN/ε where ε is the dielectric permittivity of the silica glass. The SON profile should resemble the profile of the frozen-in electric field through $\chi^{(2)} = 3\chi^{(3)}E_{\text{frozen}}$, with the assumption of a constant $\chi^{(3)}$ in the depletion region.

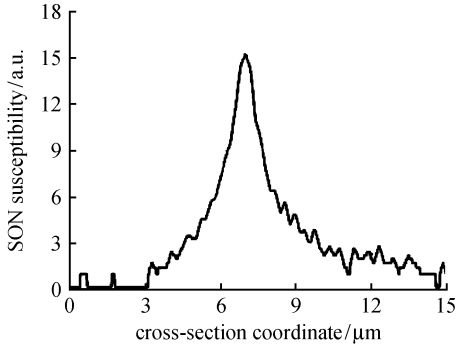

Fig. 2 Spatial distribution of SON layer

This analysis was repeated for more samples poled at 3.5 kV and 280°C for different durations. By calibrating with a quartz plate, the d_{33} is measured to be 0.3–0.5 pm/V. The centre of the SON layer is ~5 μm under the anode for 30 min. With increasing poling time, the SON layer moves deeper into the material, as shown in Fig. 3, consistent with the model of H^+ moving in from the anode.

2.3 SON in borosilicate glasses

The stability of the induced SON is a very important consideration for practical applications. It is directly related to the space-charge recombination process, which is governed by charge diffusion and field-driven migration

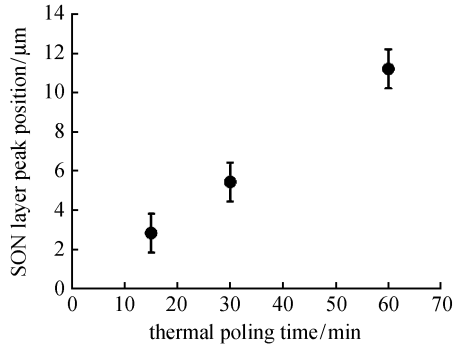

Fig. 3 Time evolution of depth of SON layer under anode in a fused silica sample thermally poled at 3.5 kV and 280°C

in the poled glasses. From this viewpoint, a glass material with higher activation energy for the migrating charge that is responsible for the annihilation of space-charge field would be preferable. Borosilicate glasses seem to fulfill this requirement and have been demonstrated to slow down charge migration and significantly enhance the SON stability in thermally poled bulk samples [12].

In 2006, An and Fleming applied the thermal poling method to a borosilicate glass (0.15-mm-thick Schott D263 microscope cover slips, with compositions by weight of 64.5% SiO_2, 6.4% Na_2O, 6.9% K_2O, 7.7% B_2O_3, 4.5% Al_2O_3, 5.9% ZnO, and 4.1% TiO_2) [13]. SON was only achieved in samples that had been poled above 1 kV, which indicated a voltage threshold. Due to a higher level of Na^+, the poling voltage had to be applied gradually, and the SON layer was only ~0.8 μm under the anode surface, as shown in Fig. 4. On the cathode surface, several crystalline phases formed (white dendrite precipitates) as a result of

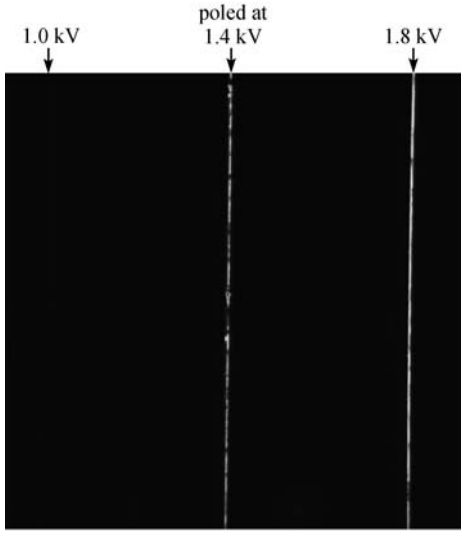

Fig. 4 SH signal from three samples of borosilicate glass poled at different voltages (image size: 375 μm×375 μm)

Na^+ ions being reduced at the cathode surface, providing strong evidence that the Na^+ ions not only migrate entirely to the cathode but can be removed from the glass (inconsistent with the "blocking electrode" assumption generally used in modeling).

2.4 SON in soda lime glasses

Soda lime silicate (SLS) glasses are attractive for optical devices since they are less expensive than fused silica but still possess excellent optical transparency and good chemical and mechanical durability. An and Fleming poled SLS glass samples at either 230°C or 280°C at 1.0–2.0 kV with electric potential increased again gradually to avoid problems due to higher conductivity [14]. SH microscopy again revealed a SON layer beneath the anode, with its intensity being lower than, but still comparable to, those observed in fused silica. A typical SH micrograph is shown in Fig. 5. The induced SON was in the range of 0.1–0.2 pm/V, with higher values expected at higher poling voltages. The layer was ~1.5 μm beneath the anode. On the cathode surface, white precipitate appeared, and by X-ray diffraction (XRD) measurement, the main crystalline phase was determined to be sodium metasilicate, $Na_2O \cdot SiO_2 \cdot nH_2O$, indicating that Na^+ ions exited the cathode surface.

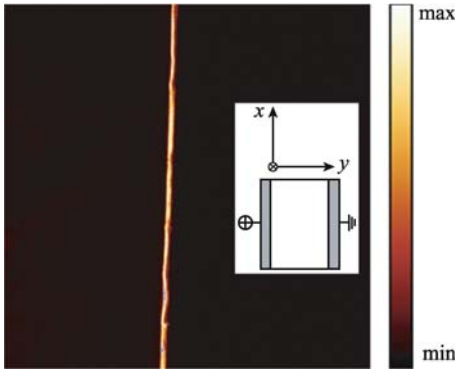

Fig. 5 Micrograph of SH signal from cross-section of SLS glass sample thermally poled at 1.8 kV and 280°C (image size is 125 μm×125 μm) (inset: schematic diagram of sample cross-section (in *x*-*y* plane) under observation)

To examine possible structural modification to the poled soda lime glass, the cross-section of the poled region was, after HF etching, observed with high-resolution scanning electron microscope (SEM), with a typical SEM micrograph as shown in Fig. 6. Below the anode surface, ~0.5 μm away from the anode edge, pillar-like features can be observed. X-ray diffraction and transmission electron microscope (TEM) measurements confirmed that these features were due to phase separation, which was found from energy dispersive spectroscopy analysis to be CaO-rich.

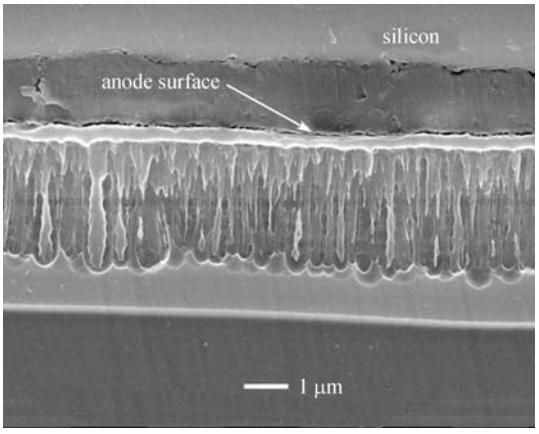

Fig. 6 SEM micrograph of HF etched cross-section of a poled soda lime glass

2.5 SON in optical fibers

Fibers used in poling are generally fabricated by the modified chemical vapor deposition (MCVD) method with Ge-doped cores. There are two types: twin-hole fiber and D-fiber, as shown in Fig. 7. Twin-hole fiber has two small holes in the cladding that run close and parallel to the core. Thin metal wires are inserted into these holes serving as electrodes. D-fiber with a single hole has one internal (inserted wire) electrode and one external electrode placed against the flat of the D-fiber. Typically, the core is closer to one electrode than the other since the SON was typically found to be located a few microns under the anode as this is where the depletion region is established. Specially prepared MCVD preforms have holes drilled in them and are drawn into fiber, typically at a relatively low temperature to avoid hole collapse. Electrodes are inserted after fiber drawing. Wong et al. developed a valuable technique involving polishing the side of the fiber until breaking through into the internal holes and then inserting the electrodes through these "side holes" [15]. Typically, electrode lengths are ~10 cm, although over 1 m is possible. Twin-hole fiber is typically poled by placing the fiber, electrodes inserted, in a small heater or on a hot plate and when the temperature has reached the required value (typically 250°C–300°C), applying a direct current (DC) voltage of typically a few kilovolts to the electrodes.

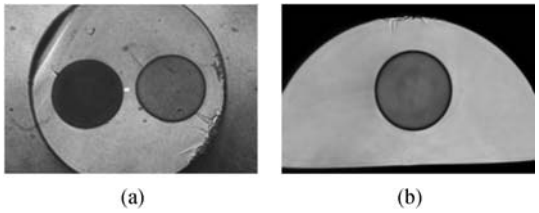

Fig. 7 Micrographs of a typical twin-hole fiber and a D-fiber. (a) Twin-hole fiber; (b) D-fiber

Typical SH micrographs are shown in Fig. 8, where Fig. 8(a) shows the fiber geometry (the potting epoxy appears brightest in the image), and Fig. 8(b) shows the SH image: the SON appears around the anode in a thin layer [16]. The depth and magnitude of d_{33} were similar to those in the planar fused silica sample. The measurement was repeated many times, and the SH signal invariably appeared as a more or less complete ring around the anode hole, indicating that the charge distributes over the glass surface. Two factors may affect the completeness of the SON ring: one is the polarization dependence on the fundamental beam, and the other is likely the randomness of the position of the closest point of the 50-μm wire to the edge of the 75-μm hole.

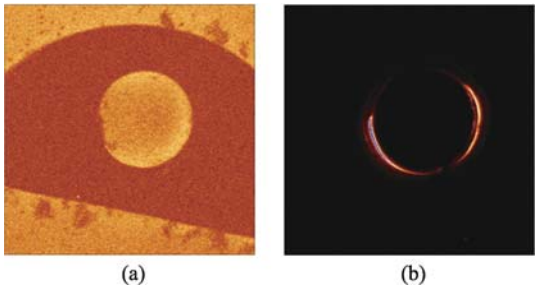

Fig. 8 SH micrographs of cross-section of a D-fiber poled at 3.5 kV and 280°C for 30 min. (a) Channel 1; (b) channel 2

The presence of a waveguiding structure results in some interesting features not observable in bulk poled silica: in the vicinity of the core, the otherwise uniform SON layer is significantly perturbed, as shown in Fig. 9. The SON layer is largely a straight line except in the vicinity of the core where it appears to be held back somewhat. This interface effect is attributed to the mismatch between the core and cladding glasses [17]. This barrier can be overcome by increasing the poling temperature and poling voltage [18].

Monitoring the time evolution of the SON layer is important for achieving optimum overlap between the SON layer and the fiber core. In 2006, An and Fleming applied SH microscopy to multiple samples of the same

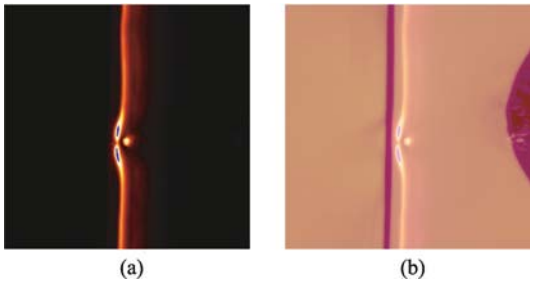

Fig. 9 SH micrographs of a D-fiber thermally poled at –2.5 kV and 280°C for 30 min. (a) Channel 2 image; (b) overlay image of Channels 1 and 2 (micrograph size is 72.5 μm×72.5 μm)

fiber poled for different durations to study the evolution of the SON layer [19]. The fiber was a standard poling D-fiber and was poled for 2, 5, 10, 20, 30, 45, and 60 min. The position and magnitude of the SON layer were measured for each poling duration, and its evolution is shown in Figs. 10 and 11. The SON layer moved essentially linearly towards the cathode with poling time (Fig. 10). The magnitude of the SON (Fig. 11) first increased with time, reached a maximum d_{33} value of ~0.32 pm/V between 5 and 20 min, and then decreased for longer poling time. At 30 min, the SON was still large (0.26 pm/V), even though the SON layer had passed through the core. A direct consequence of this observation is that poling fiber does not need to have the core in the close vicinity of the anode hole, making it easier to fabricate and further helping reduce optical loss induced by the interaction of the metal wire with the guided mode field. Fiber with a centered core was made and poled, and SH microscopy revealed a strong SON in the core [20].

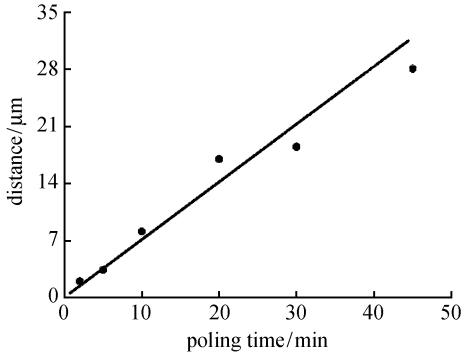

Fig. 10 Evolution of spatial distribution of SON layer

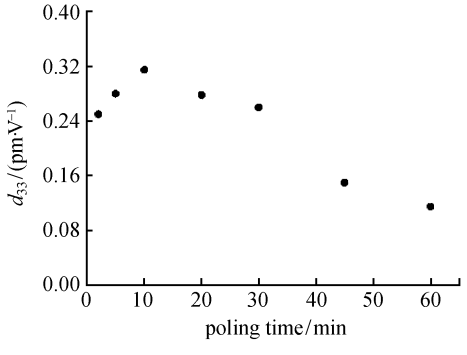

Fig. 11 Evolution of magnitude of nonlinear coefficient of SON layer

2.6 SON in laser-written waveguides

In the past several years, femtosecond laser pulses have been successfully used to directly write microstructures in transparent materials through a multiphoton absorption process, and low-loss waveguides have been obtained in optical glasses [21,22]. It would be scientifically interesting and technologically important to investigate the feasibility of inducing SON in these femtosecond laser-written optical waveguides. Thermal poling of a silica glass pre-modified by femtosecond laser irradiation was first reported in 2002 [23]. Recently, an electro-optic (EO) waveguide modulator fabricated in fused silica by a combination of femtosecond laser direct writing and thermal poling has been demonstrated [24]. To gain more experimental evidence of the feasibility, An and Fleming et al. carefully characterized the SON in thermally poled fused silica with microstructures written by femtosecond laser pulses [25]. The glass samples used were Corning 7980 synthetic flame-fused silica plates. Parallel lines of microstructures were written in the bulk of the fused silica plates by scanning with a focused beam from a mode-locked Ti:sapphire laser operating at 771 nm with a repetition rate of 250–500 kHz and pulse duration of 150 fs. The pulse energy ranged from 160 to 300 nJ per pulse, and the scanning speed varied from 50 to 500 μm/s. All written lines are in a plane parallel to the surface of the silica plate, ~12–25 μm beneath the surface. For silica plates with modified structures more than 15 μm beneath the surface, hydrofluoric acid etching was used to make the plates thinner until the written structures were < 15 μm beneath the surface to ensure an effective overlap between the laser-written structures and the thermal poling induced nonlinear region. Typical white-light optical microscopy images of the laser-written structures are shown in Fig. 12. The line spacing is 100 μm. The femtosecond laser pulses propagate from left to right in Fig. 12(b). The end-face micrograph clearly indicates that waveguiding structures have been successfully fabricated in the silica plate. The dark region behind the light-guiding region is caused by significant structural irregularities in the laser-modified region, probably caused by micro-explosions [26]. Thermal poling was carried out in air with pressed-on electrodes at 3.5 kV and 280°C for 70–100 min, with the exact poling duration being determined by the depth of the written microstructures in the silica plates. After poling, the spatial profile of the SON was investigated through directly visualizing the distribution of the generated SH signals from the poled samples using SH microscopy. In

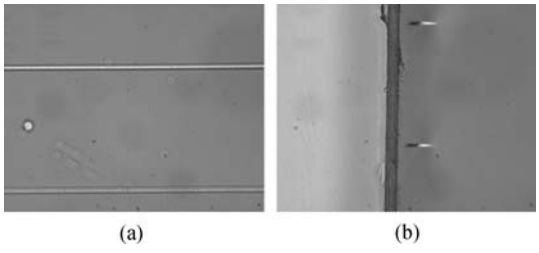

Fig. 12 Light microscopy images of laser-written filamentary structures in Corning 7980 silica plates. (a) Top view; (b) side view

the measurement, the samples were rotated so that the polarization direction of the fundamental laser beam was parallel to the poling direction to utilize the larger nonlinearity component d_{33}.

For samples poled for 70 min, the SON layer is ~9.4 μm beneath the anode silica surface and did not reach the waveguiding region. The SON magnitude d_{33}, ~0.07–0.1 pm/V, is also lower than that in fused quartz.

In order to overlap the SON layer with the laser-written waveguides, a longer poling time of 100 min was chosen. Before poling, these silica plates were processed as before, however, with an additional step. One half-section was annealed in air at 600°C for ~4 hours in an attempt to introduce and re-distribute some alkali ions to the annealed plates, since these ions are known to play an important role in poling. It was suspected that their scarcity in fused silica might hinder poling. Both halves were then identically poled. Typical SH micrographs from the polished cross-section of these samples are shown in Fig. 13. By measuring the positions of the waveguides and SON layers, it is clear that the SON layer has now reached the waveguides in both samples, being ~3.1 μm and ~2.7 μm into the waveguide for the un-annealed and annealed samples, respectively. The SON layer is weaker in the waveguiding regions than that outside the laser-modified region in both samples. The d_{33} in the waveguide was measured to be at least 1.9 times lower than that outside the waveguide. It was also observed that the SON layer around the waveguides seems to lag behind that further away from the laser-modified region, which is straight and uniform, indicating a decreased mobility for alkali ions in this region. This is expected since the laser-written waveguide is a direct result of a denser glass network induced by femtosecond irradiation, making it more difficult for alkali ions to migrate through this region. The SON ratio in the annealed and un-annealed samples has been estimated to be in the range of 1.6–2.5. This increase is attributed to a higher concentration of mobile alkali ions in the annealed sample, with surface contamination due to handling as the primary source.

A possible cause of the rather weak SON achieved in the laser-written waveguides was the potential blocking effect from regions of micro-explosion which lay in the migration path of the mobile charges. To circumvent this problem, a back-written configuration was adopted. Typical waveguides written this way with pulses of 400 nJ are shown in Fig. 14. Now, the waveguiding region is in front of the dark region supposed to be caused by micro-explosion. The tip of the laser-written structures starts ~3.0 μm from the anode surface. Thermal poling was then conducted on these waveguides, and typical result from SH microscopy is shown in Fig. 15. The SON layer, ~6.5–7.5 μm away from the anode surface, is now within the waveguiding region (refractive-index enhanced region which is brighter in the light microscope graph) but still not reaching the dark micro-explosion region. It can be seen that the SON layer is broken in the waveguiding region, showing no or very weak nonlinearity within waveguides.

We tentatively attribute the absence of SON in the laser-modified region to a more compact glass network there. The femtosecond laser-written waveguide is a direct result of denser glass structure. Lower mobility for alkali ions and other charges within this densified glass region is expected, making it more difficult for relevant ions to either enter or leave this modified region to form the frozen-in space-charge field. Heat-accumulation effects during laser irradiation may also play a role in driving out the alkali ions from the focal volume. To test this

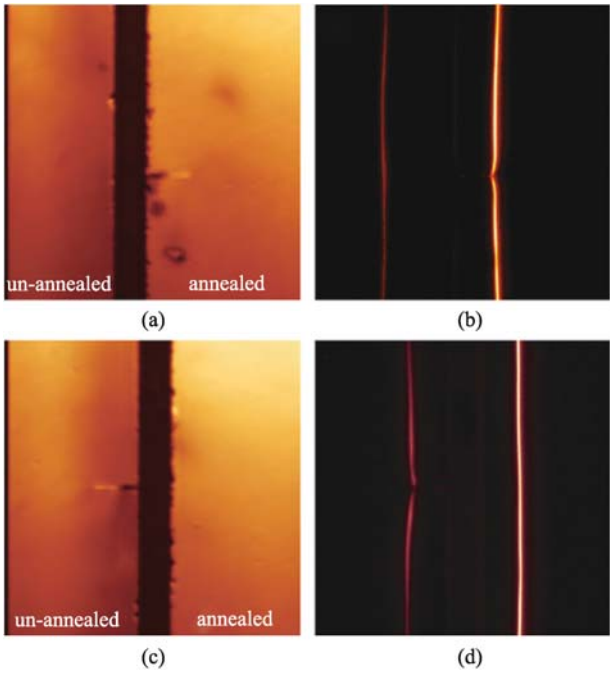

Fig. 13 Distribution of SH light in femtosecond laser modified Corning 7980 silica thermally poled for 100 min. (a) and (c) are ordinary transmission images, while (b) and (d) are SH images

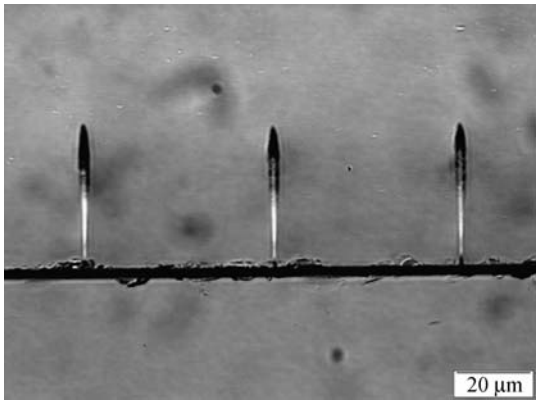

Fig. 14 Micrographs of back-written optical waveguides in silica (writing laser pulses come from the top of micrograph)

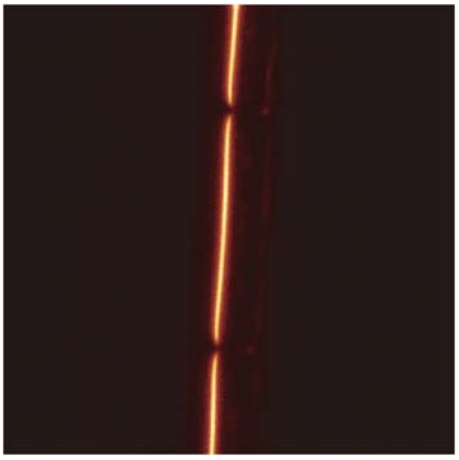

Fig. 15 SH micrograph from a thermally poled Corning 7980 silica with waveguides written by femtosecond laser pulses in back-writing configuration

hypothesis, a soda lime glass was chosen, and the distribution of alkali ions in the modified region written by a Spitfire Ti:sapphire laser (800-nm wavelength, 1-kHz repetition rate, 120-fs pulse duration, ~1.2-μJ pulse energy, 50-μm/s scanning speed, and 0.25-NA focusing lens) was measured with energy dispersive X-ray spectrometry (EDS). No attempt was made on fused silica samples because the level of alkali ions is below the limit of the EDS measurement. The result from a line scan across the modified region is shown in Fig. 16. For easy identification of the modified region under SEM, the polished surface was slightly etched in diluted hydrofluoric acid. Element Si is shown as a reference. It is clear that the concentration of Na has decreased in the laser-modified region, while Ca stays almost unchanged. This result provides indirect support to the hypothesis of a lower level of Na in the laser-modified region in fused silica. Further experiments are needed to fully resolve this issue.

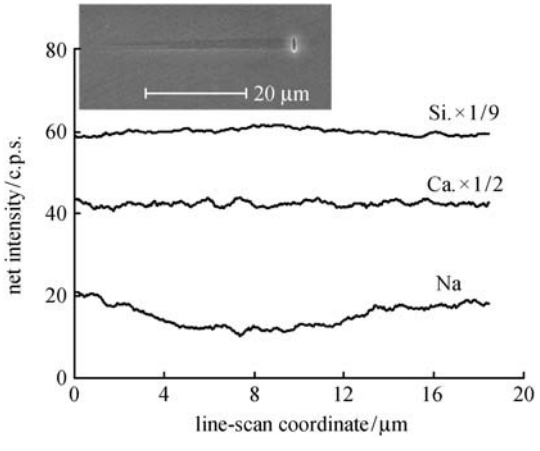

Fig. 16 Distribution of chemical elements within modified region of soda lime glass by femtosecond laser irradiation (inset is an SEM image of modified region)

3 Conclusions

The development of the understanding and technology of poling over the last twenty years has been significant. However, there is still plenty yet to be explained regarding the mechanisms, and true commercial application is still in the future. We have a very good understanding of many aspects of the mechanisms involved, and the space-charge field model is widely accepted. There is reasonable understanding of the charges involved in this process and the influence of the glass and dopants on their mobility. For the most common materials, we have a good understanding of the conditions necessary to optimize the poling process. However, there is still more to be learned before we approach a full understanding. Nevertheless, even at the current level of development, some applications appear commercially realistic. Further research has potential for commercially viable low-cost modulators and tunable gratings for telecommunications, for new sensor systems and for practical new laser sources at wavelengths otherwise not readily available.

Acknowledgements This review paper reports the work of many researchers. However, we particularly thank the staff and students, present and past, who have worked with us at OFTC on various poling research projects, and the agencies that have supported this work. The authors acknowledge the facilities as well as scientific and technical assistance from staff in the NANO Major National Research Facility at the Electron Microscope Unit, the University of Sydney.

References

1. Myers R A, Mukherjee N, Brueck S R J. Large second-order nonlinearity in poled fused silica. Optics Letters, 1991, 16(22): 1732–1734
2. Alley T G, Brueck S R J, Myers R A. Space charge dynamics in thermally poled fused silica. Journal of Non-Crystalline Solids, 1998, 242(2–3): 165–176
3. Kazansky P G, Russell P St J. Thermally poled glass: frozen-in electric field or oriented dipoles? Optics Communications, 1994, 110(5–6): 611–614
4. Fujiwara T, Wong D, Zhao Y, Fleming S, Poole S, Sceats M. Electro-optic modulation in a germanosilicate fibre with UV-excited poling. Electronics Letters, 1995, 31(7): 573–575
5. Okada A, Ishii K, Mito K, Sasaki K. Phase-matched second-harmonic generation in novel corona poled glass waveguides. Applied Physics Letters, 1992, 60(23): 2853–2855
6. Kazansky P G, Kamal A, Russell P St J. High second order nonlinearities induced in lead silicate glass by electron beam irradiation. Optics Letters, 1993, 18(9): 693–695
7. Henry L J, McGrath B V, Alley T G, Kester J J. Optical nonlinearity

in fused silica by proton implantation. Journal of the Optical Society of America B: Optical Physics, 1996, 13(5): 827–836
8. Alley T G, Brueck S R J. Visualization of the nonlinear optical space-charge region of bulk thermally poled fused-silica glass. Optics Letters, 1998, 23(15): 1170–1172
9. Margulis W, Laurell F. Interferometric study of poled glass under etching. Optics Letters, 1996, 21(21): 1786–1788
10. Kudlinksi A, Quiquempois Y, Lelek M, Zeghlache H, Martinelli G. Complete characterization of the nonlinear spatial distribution induced in poled silica glass with a submicron resolution. Applied Physics Letters, 2003, 83(17): 3623–3625
11. An H, Fleming S, Cox G. Visualization of second-order nonlinear layer in thermally poled fused silica glass. Applied Physics Letters, 2004, 85(24): 5819–5821
12. Deparis O, Corbari C, Kazansky P G, Sakaguchi K. Enhanced stability of the second-order optical nonlinearity in poled glasses. Applied Physics Letters, 2004, 84(24): 4857–4859
13. An H, Fleming S. Second-order optical nonlinearity in thermally poled borosilicate glass. Applied Physics Letters, 2006, 89(18): 181111
14. An H, Fleming S. Second-order optical nonlinearity and accompanying near-surface structural modifications in thermally poled soda-lime silicate glasses. Journal of the Optical Society of America B: Optical Physics, 2006, 23(11): 2303–2309
15. Wong D, Xu W, Fleming S, Janos M, Lo K-M. Frozen-in electrical field in thermally poled fibers. Optical Fiber Technology, 1999, 5(2): 235–241
16. An H, Fleming S. Characterization of a second-order nonlinear layer profile in thermally poled optical fibers with second-harmonic microscopy. Optics Letters, 2005, 30(8): 866–868
17. An H, Fleming S. Hindering effect of the core-cladding interface on the progression of the second-order nonlinearity layer in thermally poled optical fibers. Applied Physics Letters, 2005, 87(10): 101108
18. An H, Fleming S. Overcoming the impeding effect of core-cladding interface on the progression of the second-order nonlinearity in thermally poled optical fibers. Applied Optics, 2006, 45(24): 6212–6217
19. An H, Fleming S. Time evolution of the second-order nonlinearity layer in thermally poled optical fiber. Applied Physics Letters, 2006, 89(23): 231105
20. An H, Fleming S. Creating large second-order nonlinearity in twin-hole optical fibre with core at the centre of the two holes. Electronics Letters, 2007, 43(4): 206–207
21. Davis K M, Miura K, Sugimoto N, Hirao K. Writing waveguides in glass with a femtosecond laser. Optics Letters, 1996, 21(21): 1729–1731
22. Schaffer C B, Brodeur A, García J F, Mazur E. Micromachining bulk glass by use of femtosecond laser pulses with nanojoule energy. Optics Letters, 2001, 26(2): 93–95
23. Corbari C, Mills J D, Deparis O, Klappauf B G, Kazansky P G. Thermal poling of glass modified by femtosecond laser irradiation. Applied Physics Letters, 2002, 81(9): 1585–1587
24. Li G, Winick K A, Said A A, Dugan M, Bado P. Waveguide electro-optic modulator in fused silica fabricated by femtosecond laser direct writing and thermal poling. Optics Letters, 2006, 31(6): 739–741
25. An H, Fleming S, McMillen B W, Chen K P, Snoke D. Thermal poling induced second-order nonlinearity in femtosecond laser-modified fused silica. Applied Physics Letters, 2008, 93(6): 061115
26. Glezer E N, Mazur E. Ultrafast-laser driven micro-explosions in transparent materials. Applied Physics Letters, 1997, 71(7): 882–884